Data Analysis for Characterizing pnCCDs

Robert Andritschke, Gisela Hartner, Robert Hartmann, Norbert Meidinger, Lothar Strüder

***Abstract*—The Max-Planck-Institute semiconductor lab develops, fabricates, tests, and qualifies pnCCDs for space and ground based applications. pnCCDs are CCDs showing high quantum efficiency up to 20 keV while delivering good spatial and energy resolution. This article describes the algorithms applied to the raw data as recorded by the data acquisition system. The main purpose of the underlying software is to qualify the individual pnCCD by measurements of monoenergetic X-ray lines, from B–K (183 eV) to Mo–Kα (17.5 keV), typically Mn–Kα (5.9 keV) under various conditions (e.g. temperature, readout speed, electrical supply voltages of the detector and electronics). Therefore characteristic parameters are determined individually for each measurement as there are read noise, gains, charge transfer efficiencies, charge splitting between neighboring pixels, energy resolution, and bad pixels while correcting for offsets, gains, charge transfer inefficiencies, non-linearities of the electronics, and while recombining the charges spread over more than one pixel. These figures are used in three ways: Firstly, operating parameters are optimized by comparing individual measurements. Secondly, the individual device is rated by combining the results of all its measurements. Thus devices can be selected for applications such as measurement setups for DESY, FLASH, or the X-ray test facility PANTER. Especially the flight modules for the X-ray astronomy mission eROSITIA will be chosen based on the key figures. Thirdly, improvements gained from detector and electronics design and production modifications are quantified closing the development loop of pnCCDs and their associated electronics.**

***Index Terms*—pnCCD, data analysis, X-ray detector, correction algorithms.**

I. Introduction

ONE of the detector types designed and fabricated at the Max-Planck-Institute semiconductor lab are pnCCDs [1], [2]. This kind of CCDs has originally been developed for astronomical X-ray telescopes, XMM–Newton [3] being the first telescope equipped with such a CCD. Seven advanced pnCCDs will be built into the X-ray telescope eROSITA [4] aboard the upcoming satellite Spectrum-Roentgen-Gamma (launch planned for 2012). Even the X-ray test facility PANTER [5] makes use of pnCCDs for qualifying X-ray mirrors such as the eROSITA ones.

The unique features of high quantum efficiency (>90% in the energy band of 0.3 to 11 keV) while showing good energy and spatial resolution (<140 eV at 5.9 keV, pixel sizes are one of 36 µm × 51 µm, 51 µm × 51 µm, 75 µm × 75 µm, or 150 µm × 150 µm) and fast readout of up to 1000 frames per second, make this detector useful for other fields of research. Measurements are performed at FLASH as an example for X-ray free electron lasers [6] and at the DESY and BESSY synchrotrons [7] confirming that the detector is capable to deliver the necessary information. Other fields utilizing pnCCDs are the use as an electron detector in a transmission electron microscope or optical applications [8]. However, the rest of the text refers solely to X-ray detection.

The semiconductor lab tests the pnCCDs, evaluates their performance, and finally selects devices according to the requirements of the application. The algorithms described here are developed to extract in detail key figures from qualification measurements as described in the following section. The software is flexible enough to be as well applied to data of different situations such as synchrotron measurements (examples will be given in section VII). In these cases event lists with corrected energies and locations of impinging photons are extracted from the raw data recorded by the data acquisition system. Depending on the experiment intensity images and spatially resolved spectra can be generated for further evaluation by the experimenter.

R. Andritschke (e-mail: randrits@ipp.mpg.de), N. Meidinger, and L. Strüder are with the Max-Planck-Institut Halbleiterlabor, Otto-Hahn-Ring 6, 81739 München, Germany and the Max-Planck-Institut für extraterrestrische Physik, Giessenbachstraße, 85748 Garching, Germany.

R. Hartmann and P. Holl are with the company PNSensor GmbH, Römerstr. 28, 80803 München, Germany and the Max-Planck-Institut Halbleiterlabor.

G. Hartner is with the Max-Planck-Institut für extraterrestrische Physik.

II. pnCCD and its readout

pnCCDs are fully depleted over their full depth of 450 µm by pn–junctions. They are backside illuminated giving 100% fill factor. Both aspects result in the high quantum efficiency for X-rays. The CCDs are frame store CCDs. They can be operated as well in frame store mode as in full frame mode. The detectors explicitly designated to X-ray applications have a thin (100 nm) aluminum light shield covering the entrance window. In the frame store area the aluminum is enhanced to 1 µm. Some of the pnCCDs have frame store areas with downsized pixels along the shift direction in order to save silicon surface.

The readout of the pnCCDs is column parallel, i.e. each column has a dedicated readout channel. Each channel consists of a preamplifier, a bandwidth limiter, a correlated double sampling stage and a sample and hold. The frontend chip (CAMEX [9]) multiplexes its outputs to one or optional two outputs. The multiplexed analog signals are connected via line drivers to the analog-to-digital converter. Once the signals are digitized, a computer takes over the data and processes it, i.e. stores them on hard disk and runs the online monitor.

III. Qualification Measurements

The qualification of pnCCDs needs a well defined input which consists of monoenergetic X-ray photons homogeneously illuminating the whole CCD. We achieve this using either a radioactive ^{55}Fe source or a X-ray tube with different targets and filters.

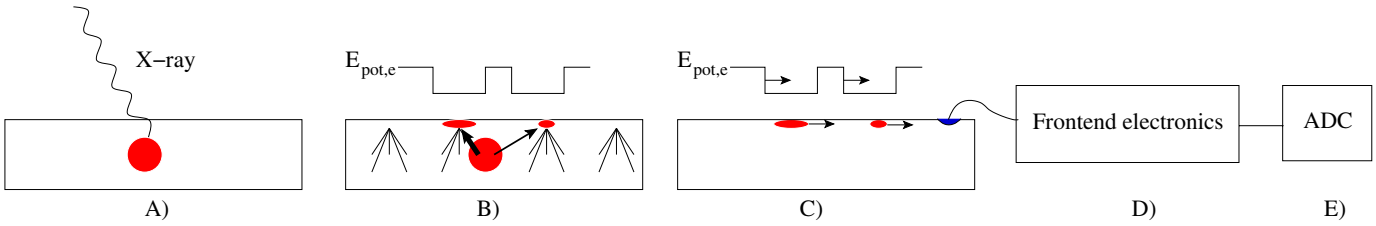

Fig. 1. Schematic of the measurement process. A) Conversion, B) storage of signal charges and leakage current, C) charge transfer to readout anode, D) frontend signal processing, E) digitization

Dark frames, i.e. frames without illuminating the CCD, are taken just before the actual measurement. This gives an on-off measurement ensuring "clean" data for calculating the offset and noise maps as described later in sections V-B and V-C.

Measurements are performed while using an online monitoring tool called Xonline which applies the same processing steps as the described "offline" software but has some algorithms simplified to run in real time.

IV. Measurement Process

In order to filter, correct, and interpret the raw data it is necessary to understand in detail the measurement process (schematically shown in Fig. 1). Not only the detector is involved in a measurement but also to a large extend the connected readout electronics. A brief overview of the successive steps from generating the charges inside the detector by an interaction of an incoming photon up to the digitizing of the resulting electrical signal should be given in the following including the distortions superimposed onto the measurement signal.

A. Absorption of Impinging X-ray Photons

Impinging X-ray photons usually interact in a photo effect resulting in a photo electron and an excited atom. The electron deposits its energy by Coulomb collisions in the semiconductor (Si) as electron–hole pairs and phonons in a statistical way introducing fluctuations in the number of generated electron–hole pairs (Fano noise). The excited atom relaxes and releases an Auger electron or a characteristic X-ray photon. The latter has a low chance to escape the detector so that in such a case the measured energy is diminished by 1.74 keV.

B. Charge Drift, Diffusion, and Collection in the Pixels

The initial charge cloud is separated in the electrical field of the bias voltage. The holes flow to the backside contact where they are absorbed. The electrons move to the pixels where they are stored in potential minima. On their way through the depleted bulk, the electron cloud widens up due to electrostatic repulsion and due to diffusion. The charge distribution has approximately a Gaussian shape. If it extends over a pixel border, the charges are collected in more than one pixel (charge splitting).

In addition, thermally generated charges are also collected in the pixels. Defects in the crystal bulk and at the surfaces can locally increase this kind of charge generation.

C. Transfer of Charges to Readout Anode

After the integration time has elapsed the charges are shifted to the readout anode. In frame store mode a quick shift from the imaging to the frame store area takes place before the readout. While shifting, a few charges can be trapped at crystal defects. Depending on the time constant a trapped charge is released early enough to keep up with the untrapped electrons, or it appears in the charge package of a successor pixel smearing out the event opposite to the shift direction. The process of losing charges is described by the charge transfer efficiency (CTE). Since it is a statistical process, it adds noise.

D. Frontend Electronics

The anode is connected to the first FET which is integrated on the detector wafer. This yields an excellent signal-to-noise factor (typically 2.2 e^- ENC noise of the overall system including the detector) since full advantage is taken from the low capacitance of the readout anode.

The analog signals of 128 channels or optional 64 channels are multiplexed to a differential output line. The multiplexed signal is guided via line drivers to the analog-to-digital converter residing in a cPCI-rack. Small, but not negligible non-linearities result from the output driver of the CAMEX frontend electronics which are improved in the current version of the CAMEX. In addition, limited bandwidths of the transmission line leads to cross talk into the successive pixel. For slow readout speeds (e.g. 50 frames/second) this effect is negligible but at fast frame rates (up to 1000 frames/second) the energy resolution worsens.

E. Digitization

Finally the digitization adds digitization noise which is usually negligible compared to the electronic and Fano noise.

V. Analysis Steps

The measurement situation is matched to the application (e.g. measured source, applied voltages to the CCD and electronics, timings). This means, that the analysis has to determine all its correction factors from the actual data set, i.e. there are not any additional measurements dedicated to calibration purposes or correction parameters being always the same.

The sequence of steps as described in the following is used in the standard analysis for the pnCCDs and deviations from that are a matter of specialized analyses. However, the software

package is flexible enough to use parameters for correction which are determined from another measurement, e.g. gain and CTE values. This way scientific measurements can be evaluated as shown in section VII.

A. Input Format for Raw Data

The data acquisition system of the pnCCDs writes a binary data format defined in-house which contains a file header and per frame a frame header followed by the complete frame data. It is important for the purpose of the analysis software to have the full information available and *not* to reduce the data since many problems can only be investigated in the full, unreduced data.

B. Offset Map

During integration of charges in the detector each pixel accumulates leakage current shifting the baseline of signals. In addition, each readout channel shows an offset. The sum of both effects is calculated by averaging pixel-by-pixel the sampled values resulting in the so-called offset map. Of course, charges generated by ionizing radiation, e.g. photons or atmospheric muons, need to be avoided. Source photons are eliminated by switching off the X-ray tube or shielding the ^{55}Fe source and taking "dark frames". Atmospheric muons need to be filtered from the data. Therefore we discard pixel-by-pixel a user supplied number (N_{mips}) of the largest values and — for symmetry — the same amount of lowest values (typically the largest and lowest 5 values for a set of 200 dark frames). Thus the offset value for a pixel (col, row) is calculated as

$$\overline{s_{\mathrm{col,row}}} = \frac{1}{N_{\mathrm{frames}} - 2 \cdot N_{\mathrm{mips}}} \cdot \left(\sum_{i \in \mathrm{frames}} s_{i,\mathrm{col,row}} - \sum_{i \in I_{\mathrm{high}}} s_{i,\mathrm{col,row}} - \sum_{i \in I_{\mathrm{low}}} s_{i,\mathrm{col,row}} \right) \quad (1)$$

with N_{frames} the number of dark frames, $s_{i,\mathrm{col,row}}$ the signal in frame i and pixel (col, row), and I_{high}, I_{low} the indices of the frames containing the N_{mips} largest and lowest values, respectively, for the corresponding pixel.

The variations between the channels dominate the structure of the offset map (Fig. 2b) and differences between pixels are not visible. Thus we calculate the so-called residual offset map. For this map the medians column-by-column and row-by-row are subtracted from the offset map revealing peculiarities of pixels.

C. Noise Map

The generation of leakage current is a statistical process resulting in noise. Another major source is the preamplifier. The dark frames are used to quantify the noise by calculating the standard deviation over these frames per pixel. The input is preprocessed in three steps: Firstly, the offset map is subtracted for practical reasons. Secondly, the same values as described for the offsets are discarded. Thirdly, the common mode noise is subtracted as described in the following section. The noise calculates as follows:

$$\sigma_{\mathrm{col,row}} = \sqrt{\frac{1}{N'_{\mathrm{frames}} - 1} \left(\sum_{i \in I_{\mathrm{sel}}} {s''_{i,\mathrm{col,row}}}^2 - N'_{\mathrm{frames}} \overline{s''_{\mathrm{col,row}}}^2 \right)} \quad (2)$$

with $N'_{\mathrm{frames}} = N_{\mathrm{frames}} - 2N_{\mathrm{mips}}$, I_{sel} all the frame indices excluding the filtered ones, and s'' the common-mode corrected signals. A noise map is shown in Fig. 2c.

For measurements without corresponding dark frames a method is implemented to calculate the offset and noise values by an running average algorithm. It is not detailed here since it is less precise and used rarely.

D. Common Mode Noise

The pnCCDs are read out column parallel. So induced noise (cross talk) affecting all channels in common (e.g. fluctuations on supply lines) imprint to the same amount on all channels of a frontend chip. This common deviation on a line-by-line basis can be calculated and subtracted. The standard algorithm calculates the median (marked with '$\sim$') of a line after offset subtraction:

$$s'_{i,\mathrm{col,row}} = s_{i,\mathrm{col,row}} - \overline{s_{i,\mathrm{col,row}}} \quad (3)$$

$$s''_{i,\mathrm{col,row}} = s'_{i,\mathrm{col,row}} - \widetilde{s'_{i,\mathrm{row}}} \quad (4)$$

This algorithm works certainly only for the case that the number of photons is less than pixels. Other algorithms can be selected for special cases but will not be described here.

E. Bad Pixels

In the noise and residual offset map bad pixels can be identified automatically. The software can find noisy pixels (i.e. pixels with increased noise) and bright pixels (i.e. pixels with highly increased leakage currents so that such a pixel can drive the electronics into saturation making the noise criterion meaningless). Pixels are marked as noisy if the calculated noise exceeds the mean noise by an user supplied factor (typically we use a factor of 2). The threshold for bright pixels is given by the user in equivalent energy per second (eV/s) and is applied to the residual offset map. The conversion to analog-to-digital converter units in which the residual offset map is expressed can certainly be done not until an energy calibration has been performed (section V-G). So this step is delayed.

In addition to the automatic recognition, the user can declare pixels as bad by means of an external text file.

F. Event Filtering, Recombination, Qualification

In all previous steps dark frames are processed. Now the photon frames are evaluated. First the events are filtered. Therefore the offset is subtracted from each frame and a common mode correction is performed as described in section V-D. Signals are discriminated against noise by applying a threshold which is a factor set by the user multiplied with the noise map (we typically use a factor of 4). The resulting pixels

over the threshold are recombined by collecting neighboring pixels in photon events (here neighbors need to share a pixel border, two pixels touching only at a corner are not classified as neighbors).

In this way an event list is formed where each event consists of one or more signals described by pixel coordinates and pulse heights (s''). Additionally the frame index and a quality value is stored with each event. The quality value encapsulates a couple of flags classifying the event:

- Border event: The event is located at one of the borders of the CCD so that potentially charges generated in the interaction are lost outside the pixel structure.
- Event containing a bad pixel
- Event next to a bad pixel: Since it is not guaranteed that charges collected in a bad pixel are measured, events in direct neighborhood of a bad pixel are marked.
- Forbidden pattern: The charge cloud has a Gaussian shape. When collected in the pixels it spreads over less than three pixels in each direction. Consequently events with a pixel pattern extending more than two pixels in one direction conflict with this assumption and are marked. As well L-shaped events with three pixels are marked if the main signal is not located at the edge.
- Overflow or Underflow event: Too large signals (e.g. caused by mips) or improper adjustments of the electronics can lead to signals extending the dynamic range of the analog-to-digital converter. Events containing such signals are marked.

G. Gain and CTE Determination and Correction

Once the event list is calculated the calibration factors can be determined. In principle the algorithm evaluates the photopeak of a monoenergetic X-ray line column-by-column (i.e. channel-by-channel) to find the gain while the slope of the peak along the rows gives the CTE. Both values were determined simultaneously in a fit. Coarse numbers were determined in advance to have good start parameters for the final fit procedure.

1) CTE Model: The model for the CTE assumes that for each shift of the signal charges from pixel to pixel a fraction of the charge is lost. One number is foreseen to describe the loss in the frame store case, two numbers in the full frame case (one number for the imaging area, the other for the frame store area since the pixel geometries of both areas can differ).

The peak position P shifts along the rows r according to

$$P(r) = \begin{cases} P_0 \cdot \mathrm{CTE}_{\mathrm{Im}}^{r} & \text{FS} \\ P_0 \cdot \mathrm{CTE}_{\mathrm{FS}}^{r} & r \leq N_{\mathrm{FS}}, \text{ FF} \\ P_0 \cdot \mathrm{CTE}_{\mathrm{FS}}^{N_{\mathrm{FS}}} \mathrm{CTE}_{\mathrm{Im}}^{r-N_{\mathrm{FS}}} & r > N_{\mathrm{FS}}, \text{ FF} \end{cases} \quad (5)$$

with $\mathrm{CTE}_{\mathrm{Im}}$ the charge transfer efficiency in the imaging area, $\mathrm{CTE}_{\mathrm{FS}}$ the one in the framestore area, N_{FS} the number of rows in the framestore area, and FS and FF denote framestore and full frame readout mode.

2) Algorithm: The ideal situation of one monoenergetic X-ray line is realizable only in some cases (e.g. synchrotron radiation). Other cases have additional lines (especially Mn-Kα and Mn-Kβ of a ^{55}Fe source, or C-K produced with a X-ray tube always produces as well O-K and a bremsstrahlung continuum). A coarse selection is done by the user since a region of interest for the energy has to be given (in units of the analog-to-digital converter). In the defined region the most prominent peak is used.

The events used in this step have to fulfill three criteria:

- All their signals are measured in the same channel since the neighboring channels have different gains. So only singles (events showing signal in only one pixel) and doubles (two pixels involved) distributed along the shift direction are usable here, whereas the doubles are only optionally allowed for the case of low photon statistics.
- The quality of the event is good; merely border events are taken into account in order to get data in the border channels as well.
- The total signal amplitude of the event is in the region of interest.

In order to prepare the CTE model fit, start parameters have to be determined and the dominant photopeak isolated.

- Coarse gains are calculated while assuming the CTE to be 1.0 (i.e. no charge transfer losses). Therefore a Gauss function is fitted to the filtered data channel-by-channel.
- These gains are applied to the data, i.e. the peaks of all channels are shifted on top of each other. The coarse gain corrected data is used to calculate a "global" CTE for the whole CCD by fitting the model (equation 5) to the data.

Based on the coarse numbers each channel runs individually through an iterative three-step process where at first the current CTE values are applied to the data (iteration 0 starts with the coarse gain and global CTE values). Then the (dominant) photo peak is isolated by fitting a Gauss function and selecting the events contained in the region of the peak position ± 3 standard deviations. Finally the model (equation 5) is fitted to the resulting data (start parameters are the current gain and a CTE of 1.0). The iteration loop is closed by taking the fitted gain as new gain and multiplying the newly fitted CTE factor to the current one. (Note that the CTE is applied already to the data and the fitted one is just a deviation!) If the gain and CTE values differ by less than 5‰ and $5 \cdot 10^{-6}$ respectively, the iteration is stopped and the final values (Fig. 2d) are applied to the data.

H. Non-linearity Factors

The spectra resulting from gain and CTE corrected data show that the photo peaks have unequal peak positions (shift is below one half width) if the data are displayed separately for the different event patterns (singles, doubles in the same channel, doubles in different channels, triples, and quadruples). Additionally, the peak widths of higher multiplicity are unexpectedly wide.

The main reason for this behavior is the slightly non-linear output driver of the frontend electronics. This has been confirmed by test pulse measurements and improved in the current version of the CAMEX readout ASIC.

The analysis optionally calculates and applies non-linearity factors. The correction is purely empirical introducing a zero order and/or a second order non-linearity factor (first order

correction is included in the gain). The zero order correction is motivated by the test pulse measurements, where a broad linear range is observed but the extrapolation does not cross the coordinate origin (it fails by typically ~ 30 adu). Thus the zero order correction subtracts a non-linearity offset value o from each of the signals an event consists of. The signal sum S of event j is calculated according to

$$S_j = \sum_i^{N_j} (s_{i,j} - o) \tag{6}$$

with N_j the number of pixels with signal in event j. If the user requests an automatic calculation of this value, the average of the shifts between the single, double, triple, and quadruple peak is returned.

The second order correction takes into account that there is a slope in the transfer function of the FEE output. It adds a quadratic term (with coefficient q) to the signals of an event:

$$S_j = \sum_i^{N_j} (s_{i,j} + q \cdot s_{i,j}^2) \tag{7}$$

The automatic calculation of the factor q assumes, that the optimal value minimizes the standard deviation of the photo peak. This optimization problem can be solved numerically by setting the first derivative of the standard deviation equal to zero and resolving for q:

$$q = \frac{\sum_i^{N_\mathrm{e}} \left(\sum_j^{N_{i,\mathrm{p}}} s_{i,j} \sum_j^{N_{i,\mathrm{p}}} s_{i,j}^2 \right) - \frac{1}{N_\mathrm{e}} \sum_i^{N_\mathrm{e}} \sum_j^{N_{i,\mathrm{p}}} s_{i,j} \cdot \sum_i^{N_\mathrm{e}} \sum_j^{N_{i,\mathrm{p}}} s_{i,j}^2}{\frac{1}{N_\mathrm{e}} \left(\sum_i^{N_\mathrm{e}} \sum_j^{N_{i,\mathrm{p}}} s_{i,j}^2 \right)^2 - \sum_i^{N_\mathrm{e}} \left(\sum_j^{N_{i,\mathrm{p}}} s_{i,j}^2 \right)^2} \tag{8}$$

with N_e the number of events and $N_{i,\mathrm{p}}$ the number of pixels with signal in event i. Since this method is sensitive on the correct selection of a monoenergetic line (crucial in the case of the measurement of a $^{55}\mathrm{Fe}$ source where the Kβ peak has to be filtered from the data) an iterative process of filtering the photopeak, calculating, and applying q is performed.

I. Outputs

The standard analysis produces a couple of plots (Fig. 2 shows selected ones) giving the experimenter the necessary information to interpret the measurement data. A short summary sheet gives an overview of the key parameters, several maps show the spatial distributions of the offsets, residual offsets, noise, bad pixels, photon intensities, and of several event pattern types. Also the gain and CTE values are visualized and the allowed event patterns and the six most prominent rejected patterns are listed including their occurence.

If the software is used to evaluate scientific data, e.g. beam measurements, event lists or intensity images can be exported.

VI. Software Implementation Details

The standard "offline" analysis is an software package consisting of several modules, each responsible for a special task, e.g. read of the raw data, offset map calculation. The parameters necessary for the analysis are supplied by the user in a parameter file, but no interactivity is implemented. Since reprocessing of measurements with changed parameters is quite common and since there are time consuming steps, e.g. the event filtering of large data sets, unnecessary processing is skipped by checking the parameters influencing the corresponding algorithms. For the ease of handling and reusability, parts of the software are encapsulated in objects, e.g. the frame reader, the event list, the bad pixels, or the gain and CTE values.

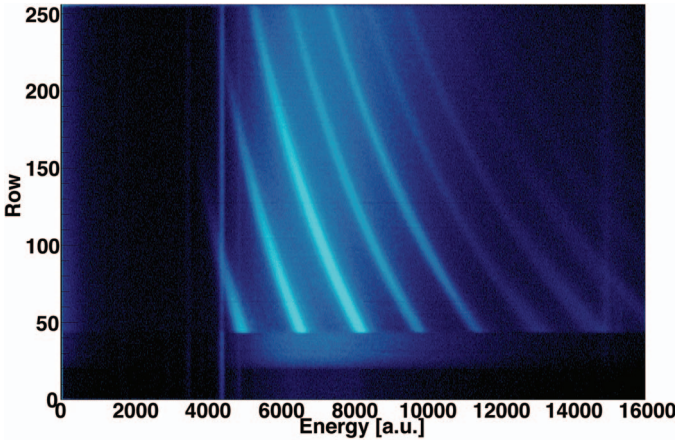

Fig. 3. Measurement at BESSY: reflection measurement of a white X-ray beam on a Cd-arachidate multilayer.

VII. Examples

A. Standard analysis of an eROSITA-sized CCD

The pnCCDs for the eROSITA X-ray telescope have a format of 384×384 pixels each in the imaging and frame store area. The pixel size is $75\,\mu\mathrm{m} \times 75\,\mu\mathrm{m}$ in the imaging area and $75\,\mu\mathrm{m} \times 51\,\mu\mathrm{m}$ in the frame store area. A selection of the output of the standard analysis is shown in Fig. 2 where a $^{55}\mathrm{Fe}$source was measured in frame store mode.

B. Evaluation of a BESSY measurement

The capability of pCCDs of simultaneously measuring position and energy is demonstrated in an experiment at the BESSY synchrotron. A white X-ray beam is directed onto a Cd-arachidat multilayer. The different energies are spread over the detector. In Fig. 3 the energy is plotted against one coordinate.

C. Evaluation of a FLASH measurement

An experiment at the FLASH free electron laser has been performed where a pulsed beam of 90 eV photons is directed onto Xe clusters. For each pulse the pnCCD reads a frame. Different scatter patterns can be found in the individual frames, one is shown in Fig. 4.

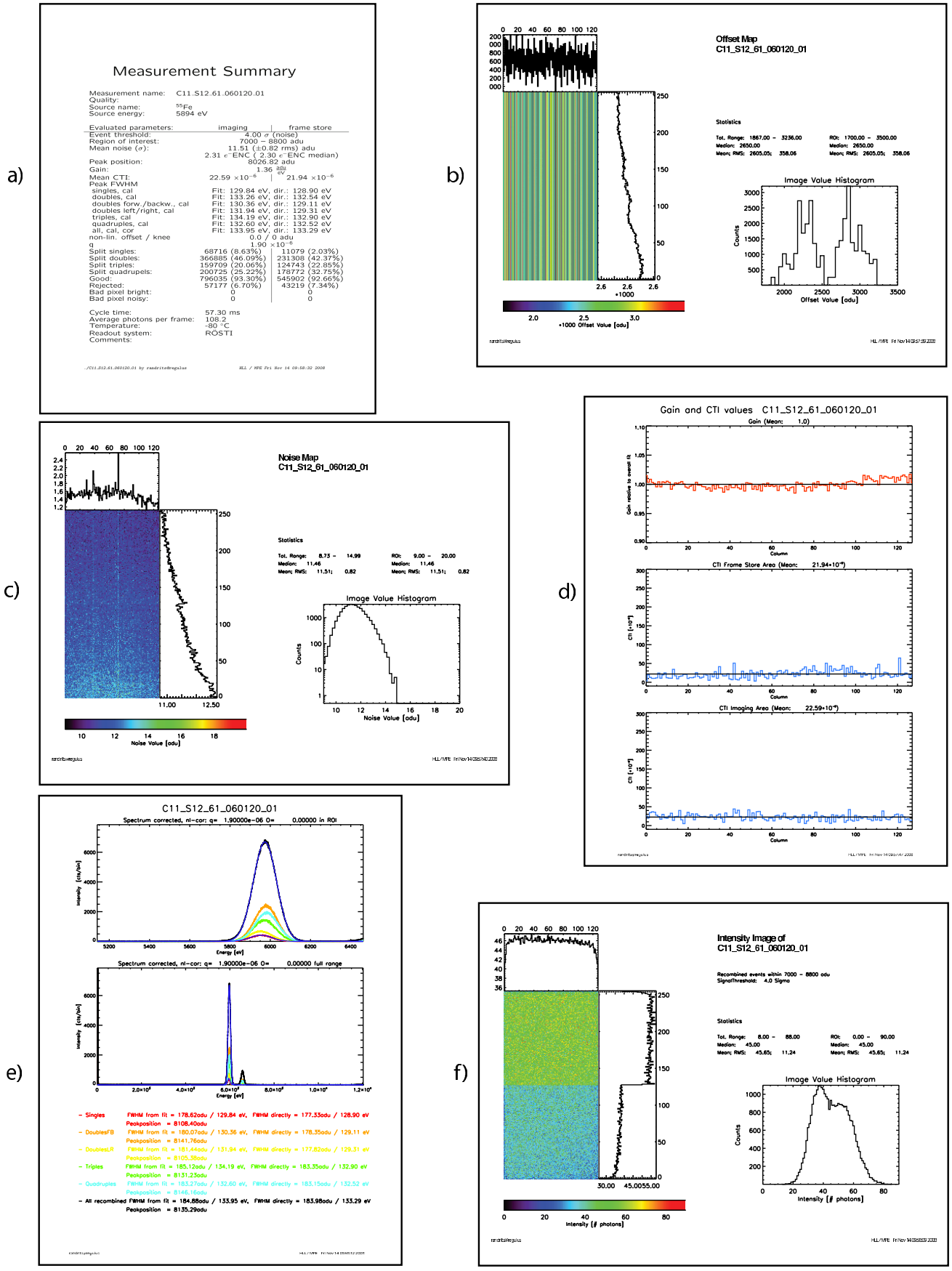

Fig. 2. Output of a standard analysis for a 128 × 128 pixel pnCCD. A ^{55}Fe source has been measured in full frame mode. a) Short summary, b) offset map, c) noise map, d) gain and CTI (charge transfer *in*efficiency values (CTI = 1 − CTE), e) corrected spectrum, f) intensity image

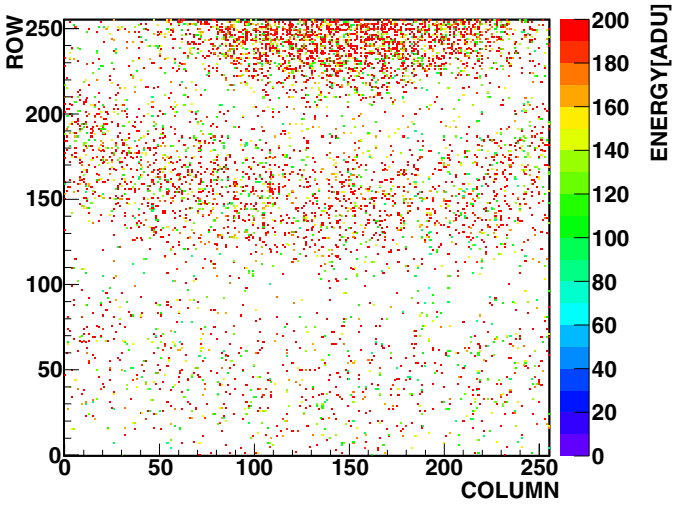

Fig. 4. Scatter image of one FLASH pulse (90 eV) impinging on Xe clusters.

VIII. Extensions and Improvements

This software has reached a mature state and is used by several people working with pnCCDs. Nevertheless some algorithms have to be refined and the software has to be adapted to new circumstances. A few examples should be mentioned briefly here:

- The correction of the non-linearity has to be investigated in greater detail.
- The CTE model has to be refined. Currently an overcompensation is observed when comparing the double events distributed along the shift direction with the perpendicular ones.
- The development of the data acquisition system targeting at the eROSITA flight electronics performs already the event filtering and reduces the data (due to limited telemetry). The input stage could be extended to handle such a reduced input as well.
- As the CCDs grow in their number of pixels the amount of data is increased. More elaborate algorithms usually need a larger number of photons to deliver superior results compared to simpler ones. So the calculation effort raises. In order to be able to take advantage of the increased power of modern computers, the algorithms have to change since not so much the instructions are executed faster, rather parallel execution in multiple CPU cores speeds up the calculations.

IX. Conclusions

As the detectors and readout electronics are improving and the number of applications increases, the requirements on the analysis grow. Lower leakage currents and higher charge transfer efficiencies lead to better energy resolutions unveiling even smaller deviations from the ideal case. Thus more detailed correction methods have to be developed and incorporated in the standard analysis so that the software keeps up with the hardware.

References

[1] N. Meidinger, R. Andritschke, R. Hartmann, S. Herrmann, P. Holl, G. Lutz, and L. Strüder, "pnCCD for photon detection from near-infrared to X-rays," *Nuclear Instruments and Methods in Physics Research A*, vol. 565, pp. 251–257, Sep. 2006.

[2] N. Meidinger, R. Andritschke, O. Hälker, R. Hartmann, G. Hasinger, S. Herrmann, P. Holl, N. Kimmel, E. Pfeffermann, P. Predehl, C. Reich, G. Schächner, H. Soltau, and L. Strüder, "Fast large-area spectroscopic and imaging CCD detectors for x-ray astronomy with eROSITA and for exploration of the nanocosmos," O. H. W. Siegmund, Ed., vol. 6686, no. 1. SPIE, 2007, p. 66860H. [Online]. Available: http://link.aip.org/link/?PSI/6686/66860H/1

[3] F. Jansen, D. Lumb, B. Altieri, J. Clavel, M. Ehle, C. Erd, C. Gabriel, M. Guainazzi, P. Gondoin, R. Much, R. Munoz, M. Santos, N. Schartel, D. Texier, and G. Vacanti, "XMM-Newton observatory. I. The spacecraft and operations," *Astronomy&Astrophysics*, vol. 365, pp. L1–L6, Jan. 2001.

[4] P. Predehl, R. Andritschke, W. Bornemann, H. Bräuninger, U. Briel, H. Brunner, W. Burkert, K. Dennerl, J. Eder, M. Freyberg, P. Friedrich, M. Fürmetz, R. Hartmann, G. Hartner, G. Hasinger, S. Herrmann, P. Holl, H. Huber, E. Kendziorra, W. Kink, N. Meidinger, S. Müller, M. Pavlinsky, E. Pfeffermann, C. Rohé, A. Santangelo, J. Schmitt, A. Schwope, M. Steinmetz, L. Strüder, R. Sunyaev, L. Tiedemann, M. Vongehr, J. Wilms, M. Erhard, S. Gutruf, D. Jugler, D. Kampf, R. Graue, O. Citterio, G. Valsecci, D. Vernani, and M. Zimmerman, "eROSITA," in *Society of Photo-Optical Instrumentation Engineers (SPIE) Conference Series*, ser. Presented at the Society of Photo-Optical Instrumentation Engineers (SPIE) Conference, vol. 6686, Sep. 2007.

[5] M. Freyberg, B. Budau, W. Burkert, G. Hartner, G. Hasinger, M. Collon, S. Kraft, M. Beijersbergen, M. Bavdaz, D. Lumb, K. Wallace, and D. Kampf, "Potential of the PANTER x-ray test facility for calibration of instrumentation for XEUS," in *Society of Photo-Optical Instrumentation Engineers (SPIE) Conference Series*, ser. Presented at the Society of Photo-Optical Instrumentation Engineers (SPIE) Conference, vol. 6266, Jul. 2006.

[6] R. Hartmann, S. Epp, S. Herrmann, P. Holl, N. Meidinger, D. Rolles, H. Soltau, L. Strüder, J. Ullrich, and G. Weidenspointner, "Large Format pnCCDs as Imaging Detectors for X-ray Free-Electron-Lasers," in *these proceedings*, no. N30-442, 2008.

[7] C. Reich, R. Hartmann, H. Soltau, L. Strüder, N. Meidinger, U. Pietsch, W. Leitenberger, C. Bostedt, and T. Möller, "Fast Spectroscopic and Imaging pnCCD Detector at BESSY and FLASH VUV-FEL," in *these proceedings*, no. N30-434, 2008.

[8] S. Ihle, R. Hartmann, M. Downing, and L. Strüder, "Optical Test Results of Fast pnCCDs," in *these proceedings*, no. N60-5, 2008.

[9] S. Herrmann, W. Buttler, R. Hartmann, N. Meidinger, M. Porro, and L. Strüder, "CAMEX readout ASIC for pnCCDs," in *these proceedings*, no. N44-4, 2008.